James C. Carr, MD
Orlando Simonetti, PhD
Jeff Bundy, PhD
Debiao Li, PhD
Scott Pereles, MD
J. Paul Finn, MD

Author contributions:
Guarantor of integrity of entire study, J.P.F.; study concepts, J.P.F., O.S., J.C.C., J.B.; study design, J.B., J.P.F., O.S., J.C.C.; literature research, J.C.C.; clinical studies, J.C.C., J.P.F., S.P.; data acquisition, J.C.C., J.P.F., D.L.; data analysis/interpretation, J.C.C., J.P.F., O.S.; statistical analysis, J.C.C., D.L.; manuscript preparation, J.C.C., J.P.F.; manuscript definition of intellectual content and editing, J.C.C., J.P.F., O.S.; manuscript revision/review and final version approval, J.P.F., O.S.

Cine MR Angiography of the Heart with Segmented True Fast Imaging with Steady-State Precession[1]

In five healthy subjects and 18 patients, cine magnetic resonance (MR) imaging of the heart was performed with a true fast imaging with steady-state precession (FISP) sequence. Results were compared both quantitatively and qualitatively with those at cine fast low-angle shot (FLASH) MR imaging. The blood-myocardial contrast-to-noise ratio (CNR) was 2.0 times higher and the normalized (for measurement time and pixel size) blood-myocardial CNR was 4.0 times higher for true FISP compared with FLASH MR imaging. Qualitative scores for image quality were significantly higher with true FISP MR imaging. Segmented cine true FISP MR imaging generated high-contrast MR images of the heart in healthy subjects and in patients with heart disease and produced image quality superior to that with cine FLASH MR imaging.

Since its introduction in 1991 (1), breath-hold cine magnetic resonance (MR) angiography has been a cornerstone for evaluation of cardiac morphology and function.

Traditionally, spoiled gradient-echo fast low-angle shot (FLASH) MR imaging has been used for cardiac cine MR angiography. However, FLASH MR imaging relies mainly on inflow enhancement to generate blood-myocardial contrast and, hence, is limited by low contrast-to-noise ratio (CNR) at short repetition time (TR) and low-flow rates. Furthermore, the longer TR required for inflow enhancement with FLASH MR imaging lengthens the acquisition time. If this flow dependence can be offset, then the dramatic shortening of the minimum TRs achiev-able with modern gradient technology can be reflected in the performance characteristics of nonenhanced MR imaging. Therefore, there is a need for a cine MR angiographic technique that can take advantage of short TRs while maintaining high intrinsic blood-myocardial contrast and blood-myocardial signal-to-noise ratio (SNR).

With true fast imaging with steady-state precession (FISP) (2–4), an alternating, large-flip-angle, radio-frequency excitation scheme coupled with a fully balanced gradient waveform is used to recycle steady-state magnetization in long T2 species. The steady-state signal is dependent on the T2-to-T1 ratio, which is relatively high for blood. This enhances signal and contrast, but the effect is dependent on maintaining coherent transverse magnetization. Factors that tend to disrupt the steady state (such as main field nonuniformity, eddy currents, and inhomogeneous magnetic susceptibility) result in off-resonance effects that manifest as dark stripes or ghosting of flow. These artifacts are more pronounced with longer TR, where image quality is unpredictable.

With recent developments in gradient hardware, TRs on the order of 3 msec are achievable with true FISP MR imaging, and the technique can be used for low-spatial-resolution, real-time evaluation of the beating heart.

The purpose of this study was to evaluate a high-spatial-resolution, segmented–k-space, true FISP MR imaging technique for cine MR angiography of the heart and to quantify its performance compared with segmented cine FLASH MR imaging in healthy subjects and patients.

Materials and Methods

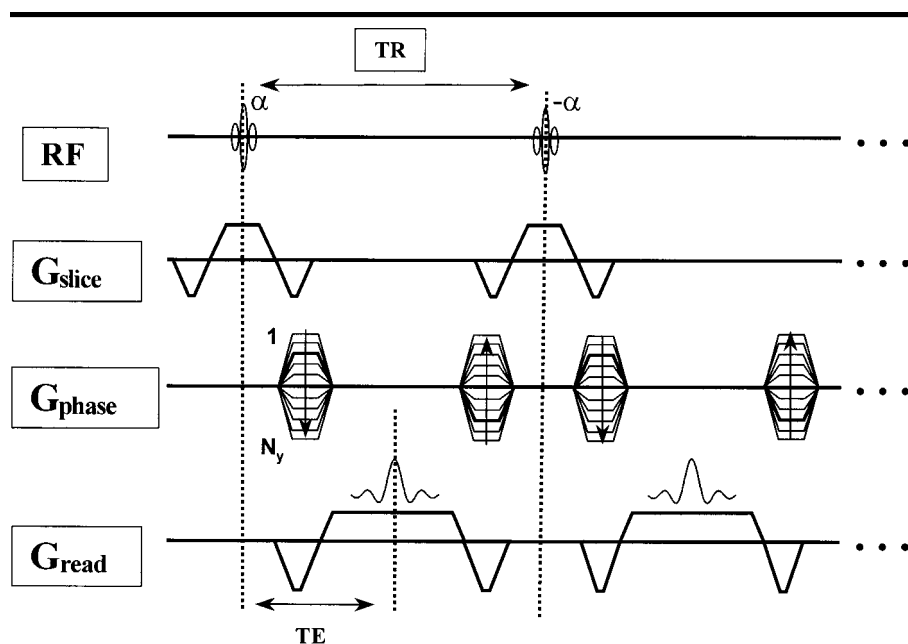Five healthy volunteers (four men and one woman; mean age, 32.6 years; age

Figure 1. Timing diagram for the true FISP pulse sequence. Transverse magnetization is maintained in the steady state from one TR to the next by rewinding the gradient (*G*) waveforms on all axes. The gradients are perfectly balanced, and the total gradient area is zero at each α radio-frequency (*RF*) pulse. *N* = number of phase-encoding steps, *TE* = echo time.

range, 24–43 years) and 18 patients (12 male and six female patients; mean age, 45.4 years; age range, 15–69 years) formed the study group. All patients had undergone echocardiography and were referred for further evaluation of clinical abnormalities. Six patients experienced aortic valve disease; one, mitral valve disease; five, left ventricular failure after myocardial infarction; one, an intramyocardial mass; one, a right-to-left shunt and Eisenmenger syndrome; one, a lung mass abutting the pericardium; one, pericardial thickening; and two, pericardial effusions. Studies were performed with a 1.5-T MR imaging system (Magnetom Sonata; Siemens Medical Systems, Iselin, NJ) with an advanced gradient system (maximum amplitude, 40 mT/m; maximum slew rate, 200 T/m/sec). Informed consent was obtained from each subject, and the study was performed in accordance with the guidelines of the institutional review board.

MR Imaging Technique

True FISP MR imaging.—A breath-hold, segmented–k-space, true FISP sequence (4) was developed for cine cardiac MR imaging. The true FISP pulse sequence is designed to maintain coherent transverse magnetization between TRs by means of balancing the gradient waveforms on all three axes so the total gradient moment is zero at each radio-frequency excitation

pulse (Fig 1). A 180° phase alternation is applied to every α radio-frequency excitation pulse. Without any special preparation, it takes approximately T1 msec for the magnetization to reach the steady state. During the approach to steady state, the magnetization oscillates around the steady-state value and induces artifacts if included in the MR image data. To prevent this, the radio frequency was pulsed for at least one cardiac cycle before data acquisition.

We implemented k-space segmentation in two versions, with 15 and 20 lines per segment, that results in a temporal frame duration of 48 and 64 msec, respectively. A linear k-space reordering scheme with no interleaving was used.

Both prospectively triggered and retrospectively gated versions were implemented. In the prospectively triggered version, a specified number of segments were acquired after each R wave trigger, depending on the R-R interval. To maintain the steady state, radio frequency and gradient pulsing continued while data acquisition ceased until the next R wave was detected. In the retrospective version, data acquisition was continuous, and the lines were sorted retrospectively, depending on their position within the cardiac cycle.

The imaging parameters for the true FISP sequence were the following: TR msec/echo time msec of 3.0/1.5, flip an-

gle of 60°, bandwidth of 975 Hz/pixel, field of view of 250–350 × 350 mm, matrix size of 120 × 256, pixel size of 2.3 × 1.4 mm, section thickness of 5 mm, acquisition time of 10 seconds, 15–20 lines per segment, no echo sharing, and effective temporal resolution of 48–64 msec.

FLASH MR imaging.—The imaging parameters for the segmented FLASH sequence were as follows: 8.0/4.0 msec, flip angle of 20°, bandwidth of 195 Hz/pixel, field of view of 250–350 × 350 mm, matrix size of 120 × 256, pixel size of 2.3 × 1.4 mm, section thickness of 6 mm, acquisition time of 15 seconds, nine lines per segment, echo sharing, and effective temporal resolution of 40 msec.

A linear interleaved trajectory was used for k-space reordering. Nine lines per segment were acquired in each R-R interval, and echo sharing was used to further decrease the effective frame duration from 72 to 40 msec.

All subjects were positioned supine on the imaging table with their arms by their sides, and they entered headfirst into the magnet. A quadrature, phased-array body coil was used, and posterior coil elements were activated to cover the thorax. Electrocardiographic electrodes were attached, and gating was obtained with four-lead electrocardiography. Subjects were asked to hold their breath in the middle of inspiration during MR imaging. To detect orientation-dependent effects, true FISP and FLASH MR images were acquired in several planes, and only those with exactly the same image orientation and section position were used for the purposes of comparison.

Quantitative Analysis

For quantitative comparison of the true FISP and FLASH sequences, 10 pairs of MR images (two long axis, five short axis, three coronal) were evaluated in the healthy subjects, and 17 pairs (nine long axis, three short axis, five coronal) were evaluated in the patients. The mean signal intensities of blood, myocardium, and background noise were measured directly by placing a circular region of interest over the relevant area in each frame of both the FLASH and true FISP series. The mean area of the region of interest for blood was 1.5 cm^2 (range, 0.3–2.8 cm^2), for myocardium was 0.46 cm^2 (range, 0.1–1.1 cm^2), and for background noise was 0.6 cm^2 (range, 0.1–1.5 cm^2). The area of the region of interest chosen for each series was the maximum permissible without causing contamination from other adjacent tissues. Because

of ventricular contraction, the region of interest was repositioned between frames. Background noise was measured at the edge of each MR image outside the chest.

The SNR for blood (SNR_b) and the SNR for myocardium (SNR_m) (1,5) were calculated with the following equations: $SNR_b = SI_b/SD_n$ and $SNR_m = SI_m/SD_n$, where SD_n is the SD of background noise, SI_b is the signal intensity of blood, and SI_m is the signal intensity of myocardium. The blood-myocardial CNR (CNR_{bm}) was calculated with the following equation: $CNR_{bm} = (SI_b - SI_m)/SD_n$.

Because of its longer TR, the acquisition time to measure a frame with FLASH MR imaging was 2.7 times greater than that with true FISP MR imaging. Echo sharing was not used in the current implementation of the segmented true FISP sequence. SNR is directly proportional to the voxel size and square root of the imaging time. To isolate the CNR performance inherent in the two sequences, the values were normalized for voxel size and measurement time (5).

The TR for true FISP MR imaging was 3 msec, and the TR for FLASH MR imaging was 8 msec. The time to produce a single frame (FT [in seconds]) in each pulse sequence was calculated with the following equation: FT = (TR × PES)/1,000, where PES is the number of phase-encoding steps.

The voxel size (VS) was calculated in cubic millimeters. The normalized CNR_{bm} (CNR_{bmN}) was calculated with the following equation: $CNR_{bmN} = CNR_{bm}/(VS \times \sqrt{FT})$. The blood-myocardial CNR and the normalized blood-myocardial CNR values were recorded for each sequence, and the mean values were calculated.

The in-plane resolution (pixel size [in square millimeters]) and acquisition time were recorded for each series.

All of the region-of-interest measurements were performed by the same observer (J.C.C.). The results for both sequences were analyzed statistically with a paired Student t test (J.C.C., J.P.F.).

Qualitative Analysis

For the purposes of qualitative comparison, 10 MR image pairs (two long axis, five short axis, three coronal) in the healthy subjects and 31 MR image pairs (14 long axis, eight short axis, six coronal, three sagittal) in the patients were assessed by two observers (J.C.C., J.P.F.), and agreement was reached by consensus. Again, each MR image pair had exactly the same section position and orientation.

The following parameters were evaluated: subjective blood-myocardial contrast, uniformity of blood signal intensity, edge definition, visualization of intracardiac structures (valve cusps, papillary muscles), visualization of pericardium, and conspicuity of any abnormality. Each parameter was scored from 1 to 5: 1, very poor; 2, poor; 3, fair; 4, good; and 5, excellent. The mean score for each parameter was calculated, and results were analyzed statistically with a paired t test.

The presence or absence of artifact was recorded. The type of artifact and orientation of the MR image on which it occurred was also noted. The severity of the artifact was graded on a scale from 1 to 3: 1, mild; 2, moderate; and 3, severe. The artifact grading system was classified as follows: mild artifact occurred on fewer than two frames and did not encroach on the region of interest; moderate artifact occurred on more than two frames and did not encroach on the region of interest; severe artifact occurred on more than two frames and did encroach on the region of interest, with potential effect on diagnosis.

❚ Results

Quantitative Analysis

The results of the quantitative analysis in the healthy subjects are given in Table 1. The mean blood SNR for true FISP imaging was higher than that for FLASH. The mean myocardial SNR for true FISP imaging was lower than that for FLASH. The blood-myocardial CNR and normalized blood-myocardial CNR were consistently higher for true FISP than for FLASH imaging for the 10 MR image pairs (Fig 2). The mean blood-myocardial CNR for true FISP imaging was 2.2 times that for FLASH (range, 1.3–4.4). The normalized mean blood-myocardial CNR for true FISP imaging was 4.12 times that for FLASH (range, 2.6–8.2).

The results of the quantitative analysis in the patients are given in Table 2. There was no significant difference in mean blood SNR between true FISP and FLASH MR imaging. The mean myocardial SNR was lower for true FISP imaging than for FLASH. The blood-myocardial CNR and normalized blood-myocardial CNR were also consistently higher for true FISP imaging than for FLASH for the 17 MR image pairs (Fig 3). The mean blood-myocardial CNR for true FISP imaging was 1.99 times that for FLASH (range, 0.99–7.11). The normalized mean blood-myocardial CNR for true FISP imaging was 3.86 times that for FLASH (range, 1.8–15.8).

The mean pixel size for true FISP imaging was 2.79 mm² (range, 1.52–5.17 mm²) and for FLASH was 3.08 mm² (range, 2.09–4.03 mm²). The mean voxel size

TABLE 1
Results of Quantitative Analysis in Healthy Subjects

Finding	True FISP Imaging	FLASH Imaging	P Value
Blood SNR	39.45	32.88	>.05
Myocardial SNR	12.99	19.92	<.01
Blood-myocardial CNR	26.49	12.96	<.001
Normalized blood-myocardial CNR (sec/mm³)	2.90	0.77	<.001
Frame time (sec)	0.52	0.98	<.001
Voxel size (mm³)	13.12	17.64	<.001

Note.—Data are the mean values.

TABLE 2
Results of Quantitative Analysis in Patients

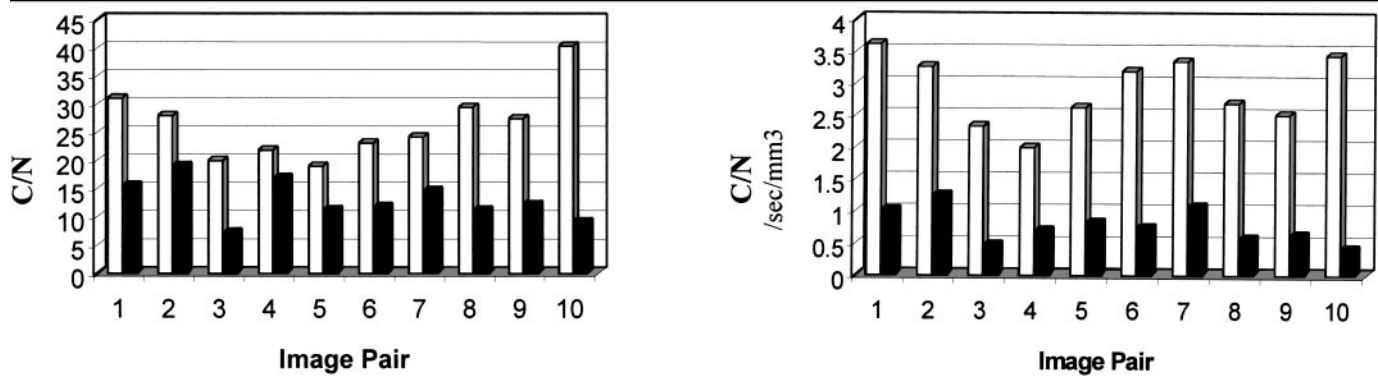| Finding	True FISP Imaging	FLASH Imaging	P Value
Blood SNR	35.29	35.10	>.05
Myocardial SNR	11.14	19.44	<.001
Blood-myocardial CNR	24.16	15.66	<.05
Normalized blood-myocardial CNR (sec/mm³)	2.59	0.84	<.001
Frame time (sec)	0.45	1.02	<.001
Voxel size (mm³)	15.25	18.61	<.001

Note.—Data are the mean values.

Figure 2. Bar graphs depict true FISP (white bars) versus FLASH (black bars) MR imaging in healthy subjects. Left: Blood-myocardial CNR (*C/N*). The mean value is more than 2.0 times higher with true FISP imaging ($P < .001$). Right: Normalized blood-myocardial CNR ($C/N/sec/mm^3$). The mean value for true FISP imaging is 4.0 times higher than that for FLASH ($P < .001$).
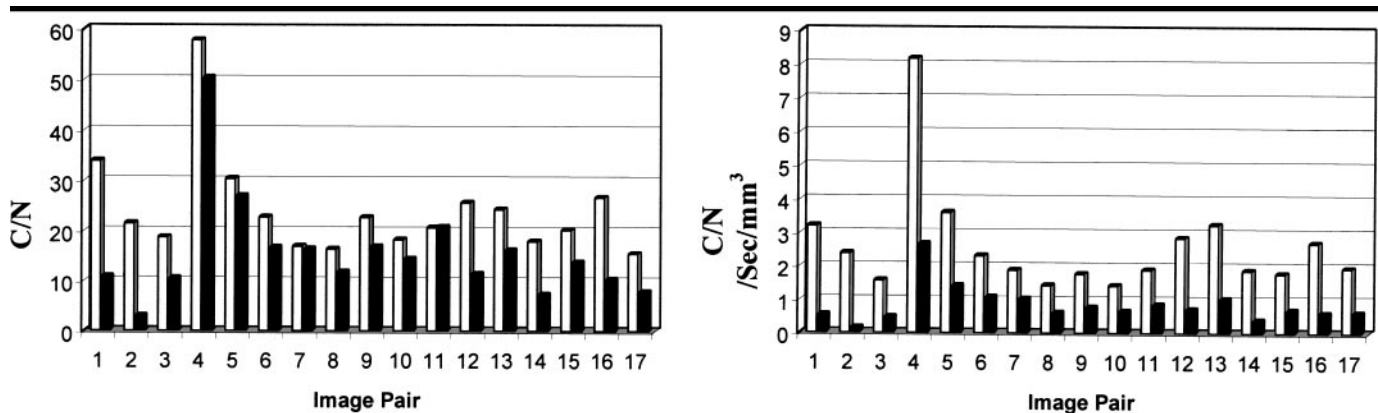

Figure 3. Bar graphs depict true FISP (white bars) versus FLASH (black bars) MR imaging in patients. Left: Blood-myocardial CNR (*C/N*). On average, the mean value is 2.0 times higher with true FISP MR imaging ($P < .05$). Right: Normalized blood-myocardial CNR ($C/N/sec/mm^3$). The mean value is, on average, 4.0 times higher with true FISP MR imaging ($P < .001$).

TABLE 3
Results of Qualitative Analysis in Healthy Subjects and Patients

Finding	True FISP Imaging	FLASH Imaging	*P* Value
Blood-myocardial contrast	4.60	3.01	<.001
Uniformity of blood signal intensity	4.09	2.93	<.001
Edge definition	4.81	2.96	<.001
Visualization*			
Valves	4.50	2.92	<.001
Papillary muscles	4.82	3.37	<.001
Pericardium	4.53	2.28	<.001
Abnormality	4.50	3.61	<.01
Severity of artifact†	1.0	0.63	>.05

Note.—Data are the mean values per participant.
  * Graded on scale of 1–5: 1, very poor; 2, poor; 3, fair; 4, good; 5, excellent.
  † Graded on scale of 1–3: 1, mild; 2, moderate; 3, severe.

was significantly smaller for true FISP imaging than for FLASH in all series.

The mean acquisition time for true FISP imaging was 10.69 seconds (range, 7.14–15.5 seconds) and for FLASH was 15.31 seconds (range, 11–21 seconds).

The mean frame time was shorter for true FISP imaging than for FLASH.

Qualitative Analysis

Ten MR image pairs in the healthy subjects (Fig 4) and 33 MR pairs in the patients, or a total of 43 MR image pairs, were assessed qualitatively (Table 3). The images of six patients had evidence of aortic regurgitation. In four of these patients, the ascending thoracic aorta was dilated. The images of one patient showed mitral regurgitation and left ventricular failure (Fig 5). The images of five patients showed poor ventricular contractility. Four of these patients had focal areas of postinfarction myocardial thinning. The images of one patient each showed a small intramyocardial mass in the interventricular septum, a patent ductus arteriosus (Fig 6), a right hilar carcinoid tumor that abutted the heart, and focal bands of pericardial thickening associated with incoordinate right ventricular contraction. Two patients had pericardial effusions.

The results of the qualitative analysis are given in Table 1. The mean scores for blood-myocardial contrast, uniformity of blood signal intensity, edge definition, and visualization of valve leaflets, papillary muscles, and pericardium were con-
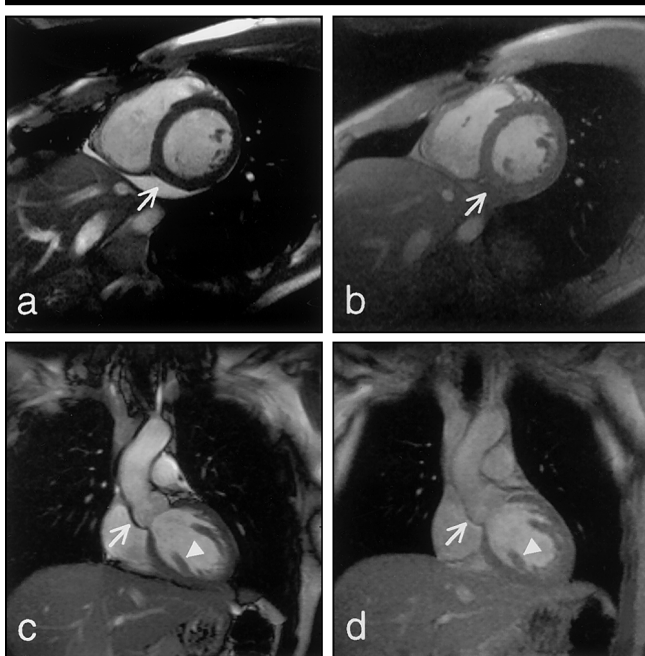
Figure 4. Healthy subject. *a*, Short-axis true FISP cine MR image demonstrates uniformly high blood signal intensity with high blood-myocardial contrast. A small amount of pericardial fluid (arrow) is visible inferiorly. *b*, Blood signal intensity and blood-myocardial contrast are reduced in the comparable FLASH MR image, and the pericardial fluid (arrow) is no longer visible. *c*, Coronal true FISP cine MR image shows good edge definition of sinuses of Valsalva (arrow) and clear visualization of papillary muscles (arrowhead). *d*, Edge definition (arrow) and visualization of papillary muscles (arrowhead) are inferior on the comparable FLASH MR image. Window settings (width, 750; center, 330) were chosen to optimize contrast appearances, and they were similar for both true FISP and FLASH MR images.

Figure 5. Left ventricular failure and mitral regurgitation. *a–c*, Three frames from a true FISP cine MR imaging series show uniform blood signal intensity (arrow) and high blood-myocardial contrast. There is evidence of mitral regurgitation (arrowhead) and a small left pleural effusion (open arrow). *d–f*, Blood signal intensity (arrow) and blood-myocardial contrast are markedly reduced on the comparable FLASH MR images. This finding illustrates the flow dependence of blood signal intensity with FLASH MR imaging. Mitral regurgitation (arrowhead) is seen again, but the pleural effusion (open arrow) is now poorly visible. Window settings (width, 750; center, 330) were chosen to optimize contrast appearances, and they were similar for both true FISP and FLASH MR images.

sistently higher for true FISP imaging than for FLASH. Abnormalities were more conspicuous with true FISP than with FLASH.

The mean score for severity of artifact was higher for true FISP imaging than for FLASH, but the difference was not significant. Severe artifact (grade 3) was seen on four true FISP image pairs compared with one FLASH pair. The mean artifact score on long-axis MR images was 1.16 for true FISP and 0.67 for FLASH; on short-axis images was 0.3 and 0, respectively; on short-axis images through the aortic root was 0.86 and 0.86, respectively; on sagittal images was 1.5 and 1.0, respectively; and on coronal images was 1.3 and 0.78, respectively.

❙ **Discussion**

The results in this study indicate that segmented cine true FISP MR imaging produces high-contrast MR images of the beating heart in healthy subjects and in patients with heart disease and can pro-

duce superior image quality compared with cine FLASH MR imaging.

Cardiac MR imaging has evolved over the years through traditional spin-echo sequences (6,7) to breath-hold fast gradient-echo sequences with FLASH imaging (8–12). Several technical advances have occurred during this time. Prospective or retrospective cardiac gating (7,13) offset the effects of cardiac motion, which permits multiphase MR imaging of cardiac contraction. With k-space segmentation (1,14,15), spatial resolution is traded for temporal resolution, and high-spatial-resolution cine MR imaging is allowed in a single breath hold. This, in turn, offsets the effects of respiratory motion.

Breath-hold cardiac cine MR imaging has traditionally been achieved with spoiled
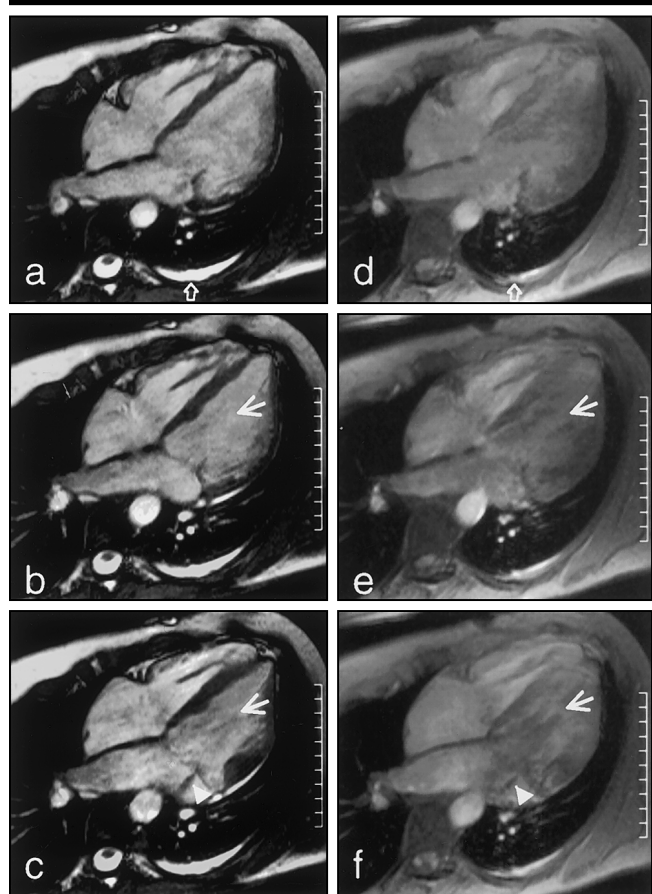
gradient-echo sequences with FLASH imaging (1). FLASH MR imaging requires a minimum TR on the order of 8 msec, not because of gradient limitations but to maintain satisfactory enhancement of inflowing blood. With improved gradient performance, the TR and acquisition time can be reduced substantially. With short TR, however, inflow enhancement and blood-myocardial contrast are compromised. Rather than rely purely on inflow enhancement, differences in the relaxation rates between blood and myocardium can be exploited by recycling transverse magnetization. This goal can be achieved with true FISP MR imaging if transverse coherence is maintained. The most obvious sequence design property of true FISP MR imaging is the zero gra-
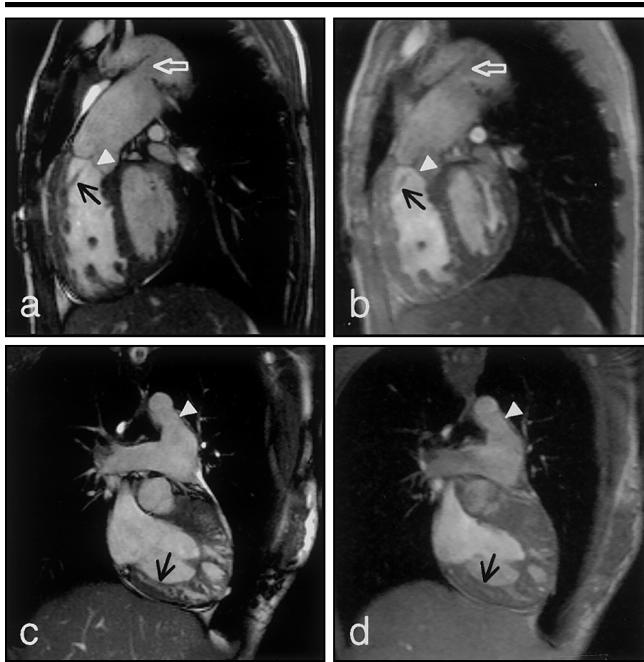
Figure 6. Patent ductus arteriosus. Sagittal *a*, true FISP and *b*, FLASH MR images demonstrate a patent ductus arteriosus (white arrow) between the pulmonary trunk and descending thoracic aorta. The pulmonary valve (arrowhead) is clearly identified, and there is pulmonary regurgitation (black arrow). Edge definition and blood-myocardial contrast are superior with true FISP MR imaging. Coronal *c*, true FISP and *d*, FLASH MR images also demonstrate the patent ductus arteriosus (arrowhead). The enlarged trabeculae (black arrow), which indicate right ventricular hypertrophy, are more conspicuous with true FISP MR imaging. The white arrow indicates the patent ductus arteriosis. Window settings (width, 660; center, 270) were chosen to optimize contrast appearances, and they were similar for both true FISP and FLASH MR images.

dient moment along all logical axes during any TR. Residual gradient moment would tend to dephase the spin system and make full recycling impossible. If there is no residual gradient moment, and the T2 of the spin system is large compared with TR, then a large portion of the residual transverse magnetization can be realigned along the main field direction by the next α radio-frequency pulse. The magnetization then becomes available for the next positive α radio-frequency excitation pulse.

If TR is large compared with the T2 of the spin system, however, substantial dephasing will occur between α radio-frequency pulses, and magnetization with a spectrum of phase histories will be generated, which gives rise to unpredictable image artifacts. The most obvious of these artifacts is a dark stripe that occurs in portions of the MR image where spins are in antiphase to each other, which cancels each signal. This phenomenon is more likely to occur when there is a steep magnetic susceptibility gradient and poor main field uniformity. If TR is long, more time is available for phase evolution in these regions, and the likelihood is greater that these regions will occur closer to the center of the field of view. In our experience, TRs more than about 5 msec are not compatible with reliable true FISP image quality, whereas reliability with TRs of 3 msec or less is increased substantially.

The FLASH pulse sequence has first-order gradient moment nulling in the section-selection and frequency-encoding directions, as is standard with bright-blood cine MR imaging. Although the true FISP sequence does not have flow compensation at the echo in the usual sense of the definition, it does have first-order gradient moment nulling during any TR and is therefore motion insensitive, insofar as the gradient waveform does not allow progressive phase accumulation.

In this study, a TR of 3 msec was used in the true FISP sequence and a TR of 8 msec in the FLASH sequence. The true FISP TR was the shortest possible TR consistent with the gradient hardware specifications. On the basis of the relative TR per line, there was an improvement in time performance of 8/3 (267%) for true FISP imaging compared with FLASH. The increased acquisition speed could be used in any combination to increase temporal resolution, increase spatial resolution, or decrease acquisition time.

With true FISP MR imaging, signal intensity increased as the flip angle increased to 60°. Constraints of the specific absorption rate limited use of flip angles above this level for cine MR imaging. Optimal image contrast was achieved at FLASH imaging with a flip angle of about 20°.

The acquisition time for true FISP imaging was significantly shorter than that for FLASH (10.69 seconds vs 15.31 seconds), and this performance was effectively doubled by means of echo sharing. Despite a much shorter acquisition time, there was no compromise in spatial resolution. This is particularly advantageous in sick patients, who have difficulty holding their breath.

Blood-myocardial CNR was twice as high for true FISP imaging than for FLASH, and normalized blood-myocardial CNR for true FISP imaging was 4.0 times that for FLASH.

The relative flow independence of true FISP signal has implications in low-flow states (eg, severe left ventricular dysfunction), where blood signal intensity and blood-myocardial contrast are reduced with FLASH MR imaging. The improved signal and contrast of true FISP MR imaging has positive implications for image segmentation in the derivation of cardiac functional parameters and left ventricular muscle mass (16).

Edge definition was superior with true FISP imaging than with FLASH, partly because of intravoxel fat-water phase cancellation due to an estimated relative fat-water phase of approximately 125°. At FLASH imaging with an echo time of 4 msec, fat and water were almost fully in phase, and the boundary between pericardium and epicardial fat was sometimes indistinct. True FISP MR images showed improved delineation of anatomic structures, including pericardium, compared with FLASH MR images. True FISP MR imaging has the potential to improve the depiction of valvular and pericardial disease, which needs to be evaluated in formal clinical studies.

True FISP MR imaging has some limitations. First, because of the requirement for a very short TR, the pulse sequence can best be implemented with high-performance gradients. Second, true FISP

MR imaging is sensitive to off-resonance effects from magnetic field nonuniformities and magnetic susceptibility gradients, which results in dark stripe artifact or ghosts of flow. These artifacts become more pronounced as the TR increases, and the lines appear closer together on the MR image. For a given resonance offset $\Delta\omega$, the phase accumulation during TR is $\phi = \Delta\omega \times TR$. When $\phi = \pi$, signal cancellation and dark stripes occur. By keeping TR low, there is less time for phase accumulation, these lines are pushed further apart, and the effect of magnetic field nonuniformity is minimized. Implanted metallic devices can result in noticeable artifact from magnetic field nonuniformity that may be partially improved by means of additional shimming of the magnet. Finally, true FISP MR imaging is affected by pulsatility artifact, particularly from the aorta and great vessels, in a manner that appears orientation dependent. In our study, artifact was more severe on MR images with orientations that included the aorta. The effect was generally limited to isolated frames in the cardiac cycle, and it rarely encroached on the region of interest to compromise the diagnostic information. The exact mechanisms that underlie this phenomenon are not yet fully understood, to our knowledge.

In conclusion, true FISP imaging consistently produces higher blood-myocardial contrast than does FLASH. Moreover, acquisition times are shortened, potentially several fold, without compromising spatial resolution. The superior image quality with true FISP MR imaging allows clearer visualization of anatomic structures and potentially may improve detection of abnormalities. Although true FISP MR imaging is more prone to artifacts than is FLASH imaging, they do not typically compromise diagnostic information.

References
1. Atkinson DJ, Edelman R. Cineangiography of the heart in a single breath hold with a segmented TurboFLASH sequence. Radiology 1991; 178:357–360.
2. Oppelt A, Graumann R, Barfuss H. FISP: a new fast MRI sequence. Electromedica 1986; 54:15–18.
3. Deimling M, Heid O. Magnetization prepared TrueFISP imaging (abstr). In: Proceedings of the Second Meeting of the Society of Magnetic Resonance 1994. Berkeley, Calif: Society of Magnetic Resonance, 1994; 495.
4. Bundy J, Simonetti O, Laub G, Finn JP. Segmented TrueFISP imaging of the heart (abstr). In: Proceedings of the Seventh Meeting of the International Society for Magnetic Resonance in Medicine. Berkeley, Calif: International Society for Magnetic Resonance in Medicine, 1999; 1282.
5. Kaufman L, Kramer DM, Crooks LE, et al. Measuring signal-to-noise ratios in MR imaging. Radiology 1989; 173:265–267.
6. Herfkens RJ, Higgins CB, Hricak H, et al. Nuclear magnetic resonance imaging of the cardiovascular system: normal and pathologic findings. Radiology 1983; 147:749–759.
7. Lanzer P, Botvinick E, Schiller NB, et al. Cardiac imaging using gated magnetic resonance. Radiology 1984; 150:121–127.
8. Frahm J, Haase A, Matthaei D. Rapid NMR imaging of dynamic processes using the FLASH technique. Magn Reson Med 1986; 3:321–327.
9. Haase A, Frahm J, Matthaei D, et al. FLASH imaging: rapid NMR imaging using low flip angle pulses. J Magn Reson 1986; 67:258–266.
10. Frahm J, Merboldt KD, Bruhn H, et al. 0.3-second FLASH MRI of the human heart. Magn Reson Med 1990; 13:150–157.
11. Chien D, Merboldt K, Hanicke W, et al. Advances in cardiac applications of sub-second FLASH MRI. Magn Reson Imaging 1990; 8:829–836.
12. Frahm J, Haase A, Matthaei D. Rapid three-dimensional MR imaging using the FLASH technique. J Comput Assist Tomogr 1986; 10:363–368.
13. Lenz G, Haacke EM, White RD. Retrospective cardiac gating: a review of technical aspects and future directions. Magn Reson Imaging 1989; 7:445–455.
14. Edelman RR, Wallner B, Singer A, et al. Segmented turbo FLASH: method for breath-hold MR imaging of the liver with flexible contrast. Radiology 1990; 177:515–521.
15. Chien D, Atkinson D, Edelman RR. Strategies to improve contrast in turboFLASH imaging: reordered phase encoding and k-space segmentation. J Magn Reson Imaging 1991; 1:63–70.
16. Fang W, Pereles FS, Bundy J, et al. Evaluating left ventricular function using real-time TrueFISP: a comparison with conventional techniques (abstr). In: Proceedings of the Eighth Meeting of the International Society for Magnetic Resonance in Medicine. Berkeley, Calif: International Society for Magnetic Resonance in Medicine, 2000; 308.